Estimate of tissue composition in malignant and benign breast lesions by time-domain optical mammography

Giovanna Quarto,[1,*] Lorenzo Spinelli,[2] Antonio Pifferi,[1,2] Alessandro Torricelli,[1] Rinaldo Cubeddu,[1,2] Francesca Abbate,[3] Nicola Balestreri,[4] Simona Menna,[3] Enrico Cassano,[3] and Paola Taroni[1,2]

[1]*Dipartimento di Fisica, Politecnico di Milano, Piazza Leonardo da Vinci 32, 20133 Milano, Italy*
[2]*Istituto di Fotonica e Nanotecnologie, Consiglio Nazionale delle Ricerche, Piazza Leonardo da Vinci 32, 20133 Milano, Italy*
[3]*European Institute of Oncology, Breast Imaging Unit, Via G. Ripamonti, 435, 20141 Milano, Italy*
[4]*European Institute of Oncology, Department of Radiology, Via G. Ripamonti, 435, 20141 Milano, Italy*
giovanna.quarto@polimi.it

Abstract: The optical characterization of malignant and benign breast lesions is presented. Time-resolved transmittance measurements were performed in the 630-1060 nm range by means of a 7-wavelength optical mammograph, providing both imaging and spectroscopy information. A total of 62 lesions were analyzed, including 33 malignant and 29 benign lesions. The characterization of breast lesions was performed applying a perturbation model based on the high-order calculation of the pathlength of photons inside the lesion, and led to the assessment of oxy- and deoxy-hemoglobin, lipids, water and collagen concentrations. Significant variations between tumor and healthy tissue were observed in terms of both absorption properties and constituents concentration. In particular, benign lesions and tumors show a statistically significant discrimination in terms of absorption at several wavelengths and also in terms of oxy-hemoglobin and collagen content.

OCIS codes: (170.5280) Photon migration; (170.6510) Spectroscopy, tissue diagnostics; (170.3830) Mammography; (170.6920) Time-resolved imaging.

References and links

1. F. Bray., P. McCarron and D. M. Parkin, "The changing global patterns of female breast cancer incidence and mortality," Breast Cancer Res. 6, 229-239 (2004).
2. http://www.cancer.gov/
3. L. Tabar, M. F. Yen, B. Vitak, H. H. Chen, R. A. Smith, and S. W. Duffy, "Mammography service screening and mortality in breast cancer patients: 20-year follow-up before and after introduction of screening," Lancet 361, 1405-1410 (2003).
4. E. Marshall, "Public health. Brawling over mammography," Science 327, 936-938 (2010).
5. K. T. Moesta, S. Fantini, H. Jess, S. Totkas, M. A. Franceschini, M. Kaschke, and P. M. Schlag, "Contrast features of breast cancer in frequency-domain laser scanning mammography," J. Biomed. Opt. 3, 129-136 (1998).
6. L. Gotz, S. H. Heywang-Kobrunner, O. Schutz, and H. Siebold, "Optical mammography in preoperative patients," Aktuelle Radiol. 8, 31-33 (1998).
7. S. Colak, M. Van der Mark, G. t Hooft, J. Hoogenraad, E. Van der Linden, and F. Kuijpers, "Clinical optical tomography and NIR spectroscopy for breast cancer detection," Selected Topics in Quantum Electronics, IEEE Journal of 5, 1143-1158 (1999).
8. H. Jiang, Y. Xu, N. Iftimia, J. Eggert, K. Klove, L. Baron, and L. Fajardo, "Three-dimensional optical tomographic imaging of breast in a human subject," IEEE Trans. Med. Imaging 20, 1334-1340 (2001).
9. T. Durduran, R. Choe, J. P. Culver, L. Zubkov, M. J. Holboke, J. Giammarco, B. Chance, and A. G. Yodh, "Bulk optical properties of healthy female breast tissue," Phys. Med. Biol. 47, 2847-2861 (2002).
10. H. Dehghani, B. W. Pogue, S. P. Poplack, and K. D. Paulsen, "Multiwavelength three-dimensional near-infrared tomography of the breast: initial simulation, phantom, and clinical results," Appl. Opt. 42, 135-145 (2003).

11. D. Grosenick, K. T. Moesta, H. Wabnitz, J. Mucke, C. Stroszczynski, R. Macdonald, P. M. Schlag, and H. Rinneberg, "Time-domain optical mammography: initial clinical results on detection and characterization of breast tumors," Appl. Opt. 42, 3170-3186 (2003).
12. X. Cheng, J. M. Mao, R. Bush, D. B. Kopans, R. H. Moore, and M. Chorlton, "Breast cancer detection by mapping hemoglobin concentration and oxygen saturation," Appl. Opt. 42, 6412-6421 (2003).
13. P. Taroni, A. Torricelli, L. Spinelli, A. Pifferi, F. Arpaia, G. Danesini, and R. Cubeddu, "Time-resolved optical mammography between 637 and 985 nm: clinical study on the detection and identification of breast lesions," Phys. Med. Biol. 50, 2469-2488 (2005).
14. J. Wang, S. Jiang, Z. Li, R. diFlorio-Alexander, R. J. Barth, P. a. Kaufman, B. W. Pogue, and K. D. Paulsen, "In vivo quantitative imaging of normal and cancerous breast tissue using broadband diffuse optical tomography," Med. Phys. **37,** 3715-3715 (2010).
15. S. Kukreti, A. E. Cerussi, W. Tanamai, D. Hsiang, B. J. Tromberg, and E. Gratton, "Characterization of metabolic differences between benign and malignant tumors: high-spectral-resolution diffuse optical spectroscopy," Radiology **254,** 277-284 (2010).
16. S. Fantini, S. A. Walker, M. A. Franceschini, M. Kaschke, P. M. Schlag, and K. T. Moesta, "Assessment of the size, position, and optical properties of breast tumors in vivo by noninvasive optical methods," Appl. Opt. 37, 1982-1989 (1998).
17. A. E. Cerussi, A. J. Berger, F. Bevilacqua, N. Shah, D. Jakubowski, J. Butler, R. F. Holcombe, and B. J. Tromberg, "Sources of absorption and scattering contrast for near-infrared optical mammography," Acad. Radiol. 8, 211-218 (2001).
18. V. Chernomordik, D. W. Hattery, D. Grosenick, H. Wabnitz, H. Rinneberg, K. T. Moesta, P. M. Schlag, and A. Gandjbakhche, "Quantification of optical properties of a breast tumor using random walk theory," J. Biomed. Opt. 7, 80-87 (2002).
19. T. O. McBride, B. W. Pogue, S. Poplack, S. Soho, W. A. Wells, S. Jiang, U. L. Osterberg, and K. D. Paulsen, "Multispectral near-infrared tomography: a case study in compensating for water and lipid content in hemoglobin imaging of the breast," J. Biomed. Opt. 7, 72-79 (2002).
20. S. Srinivasan, B. W. Pogue, S. Jiang, H. Dehghani, C. Kogel, S. Soho, J. J. Gibson, T. D. Tosteson, S. P. Poplack, and K. D. Paulsen, "Interpreting hemoglobin and water concentration, oxygen saturation, and scattering measured in vivo by near-infrared breast tomography," Proc. Natl. Acad. Sci. U. S. A. 100, 12349-12354 (2003).
21. Q. Zhu, E. B. Cronin, A. A. Currier, H. S. Vine, M. Huang, N. Chen, and C. Xu, "Benign versus malignant breast masses: optical differentiation with US-guided optical imaging reconstruction," Radiology 237**,** 57-66 (2005).
22. Q. Zhu, P. U. Hegde, A. Ricci Jr, M. Kane, E. B. Cronin, Y. Ardeshirpour, C. Xu, A. Aguirre, S. H. Kurtzman, P. J. Deckers, and S. H. Tannenbaum, "Early-stage invasive breast cancers: potential role of optical tomography with US localization in assisting diagnosis," Radiology 256, 367-378 (2010).
23. D. Grosenick, H. Wabnitz, K. T. Moesta, J. Mucke, M. Moller, C. Stroszczynski, J. Stossel, B. Wassermann, P. M. Schlag, and H. Rinneberg, "Concentration and oxygen saturation of haemoglobin of 50 breast tumours determined by time-domain optical mammography," Phys. Med. Biol. 49, 1165-1181 (2004).
24. L. Spinelli, A. Torricelli, A. Pifferi, P. Taroni, G. Danesini, and R. Cubeddu, "Characterization of female breast lesions from multi-wavelength time-resolved optical mammography," Phys. Med. Biol. 50, 2489-2502 (2005).
25. A. Cerussi, N. Shah, D. Hsiang, A. Durkin, J. Butler, and B. J. Tromberg, "In vivo absorption, scattering, and physiologic properties of 58 malignant breast tumors determined by broadband diffuse optical spectroscopy," J. Biomed. Opt. 11, 044005 (2006).
26. D. V. van, S. Elias, A. Wiethoff, d. V. van, A. Leproux, T. Nielsen, B. Brendel, L. Bakker, d. M. van, W. Mali, and P. Luijten, "Diffuse optical tomography of the breast: initial validation in benign cysts," Molecular imaging and biology : MIB : the official publication of the Academy of Molecular Imaging 11, 64-70 (2009).
27. J. Wang, S. Jiang, Z. Li, R. diFlorio-Alexander, R. J. Barth, P. a. Kaufman, B. W. Pogue, and K. D. Paulsen, "In vivo quantitative imaging of normal and cancerous breast tissue using broadband diffuse optical tomography," Med. Phys. 37, 3715-3715 (2010).
28. S. a. Carp, A. Y. Sajjadi, C. M. Wanyo, Q. Fang, M. C. Specht, L. Schapira, B. Moy, A. Bardia, D. a. Boas, and S. J. Isakoff, "Hemodynamic signature of breast cancer under fractional mammographic compression using a dynamic diffuse optical tomography system," Biomedical optics express 4, 2911-24 (2013).
29. M. L. Flexman, H. K. Kim, J. E. Gunther, E. A. Lim, M. C. Alvarez, E. Desperito, K. Kalinsky, D. L. Hershman, and A. H. Hielscher, "Optical biomarkers for breast cancer derived from dynamic diffuse optical tomography," J. Biomed. Opt. 18, 096012 (2013).
30. A. M. Laughney, V. Krishnaswamy, E. J. Rizzo, M. C. Schwab, R. J. Barth Jr, D. J. Cuccia, B. J. Tromberg, K. D. Paulsen, B. W. Pogue, and W. A. Wells, "Spectral discrimination of breast pathologies in situ using spatial frequency domain imaging," Breast Cancer Res. 15, R61 (2013).
31. A. Lochter and M. J. Bissell, "Involvement of extracellular matrix constituents in breast cancer," Semin. Cancer Biol. **6,** 165-173 (1995).
32. P. P. Provenzano, D. R. Inman, K. W. Eliceiri, J. G. Knittel, L. Yan, C. T. Rueden, J. G. White, and P. J. Keely, "Collagen density promotes mammary tumor initiation and progression," BMC medicine **6,** 11-11 (2008).

33. A. Sassaroli, F. Martelli, and S. Fantini, "Perturbation theory for the diffusion equation by use of the moments of the generalized temporal point-spread function. I. Theory," J. Opt. Soc. Am. A Opt. Image Sci. Vis. 23, 2105-2118 (2006).
34. P. Taroni, A. Pifferi, E. Salvagnini, L. Spinelli, A. Torricelli, and R. Cubeddu, "Seven-wavelength time-resolved optical mammography extending beyond 1000 nm for breast collagen quantification," Opt. Express 17, 15932-15946 (2009).
35. C. D'Andrea, L. Spinelli, A. Bassi, A. Giusto, D. Contini, J. Swartling, A. Torricelli, and R. Cubeddu, "Time-resolved spectrally constrained method for the quantification of chromophore concentrations and scattering parameters in diffusing media," Opt. Express 14, 1888-1898 (2006).
36. M. S. Patterson, B. Chance, and B. C. Wilson, "Time resolved reflectance and transmittance for the non-invasive measurement of tissue optical properties," Appl. Opt. 28, 2331-2336 (1989).
37. R. C. Haskell, L. O. Svaasand, T. T. Tsay, T. C. Feng, M. S. McAdams, and B. J. Tromberg, "Boundary conditions for the diffusion equation in radiative transfer," J. Opt. Soc. Am. A Opt. Image Sci. Vis. 11, 2727-2741 (1994).
38. J. R. Mourant, T. Fuselier, J. Boyer, T. M. Johnson, and I. J. Bigio, "Predictions and measurements of scattering and absorption over broad wavelength ranges in tissue phantoms," Appl. Opt. 36, 949-957 (1997).
39. A. M. Nilsson, C. Sturesson, D. L. Liu, and S. Andersson-Engels, "Changes in spectral shape of tissue optical properties in conjunction with laser-induced thermotherapy," Appl. Opt. 37, 1256-1267 (1998).
40. S. Del Bianco, F. Martelli and G. Zaccanti, "Penetration depth of light re-emitted by a diffusive medium: theoretical and experimental investigation," Phys. Med. Biol. 47, 4131–4144 (2002).
41. D. Grosenick, H. Wabnitz, H. Rinneberg, K. T. Moesta, and P.Schlag, "Development of a time-domain optical mammograph and first in vivo applications," Appl. Opt. 38, 2927–2943 (1999).
42. L. Zucchelli, D. Contini, R. Re, A. Torricelli and L. Spinelli, "Method for the discrimination of superficial and deep absorption variations by time domain fNIRS," Biomed. Opt. Express 4, 2893-2910 (2013).
43. P. Taroni, A. Pifferi, G. Quarto, L. Spinelli, A. Torricelli, F. Abbate, A. Villa, N. Balestreri, S. Menna, E. Cassano, and R. Cubeddu, "Noninvasive assessment of breast cancer risk using time-resolved diffuse optical spectroscopy," J. Biomed. Opt. 15, 060501 (2010).
44. P. Taroni, G. Quarto, A. Pifferi, F. Ieva, A. M. Paganoni, F. Abbate, N. Balestreri, S. Menna, E. Cassano, and R. Cubeddu, "Optical identification of subjects at high risk for developing breast cancer," J. Biomed. Opt. 18, 060507 (2013).
45. H. Wabnitz, A. Jelzow, M. Mazurenka, O. Steinkellner, R. Macdonald, A. Pifferi, A. Torricelli, D. Contini, L. M. G. Zucchelli, L. Spinelli, R. Cubeddu, D. Milej, N. Zolek, M. Kacprzak, P. Sawosz, A. Liebert, S. Magazov, J. C. Hebden, F. Martelli, P. Di Ninni, and G. Zaccanti, "Performance assessment of time-domain optical brain imagers: a multi-laboratory study," Proc.SPIE 8583, 85830-85830-14 (2013).

1. Introduction

Breast cancer is one of the most common tumors and one of the leading causes of death in women [1]. According to estimates of lifetime risk by the U.S. National Cancer Institute [2], in the U.S. 1 in 8 women will develop breast cancer in their lifetime.

Many countries (*e.g.* U.K., Italy, Australia) offer screening programs to women for prevention, typically between 50 and 70 years of age, since early diagnosis and consequent therapy significantly reduces mortality and could improve the quality of life [3]. Breast screening essentially relies on X-ray mammography, which is the first line of defense in the early diagnosis of the breast cancer. However, mammography is less accurate in patients with dense glandular breasts [4], including young women, with reported sensitivity as low as 48%.

Optical mammography is an interesting emerging diagnostic tool which can operate at multiple wavelengths so as to combine imaging and spectroscopic information for lesion detection and characterization at the same time. In addition to its non-invasive nature, optical mammography has the capability to investigate dense breasts, typical of young women. Breast lesion characterization by non-invasive optical means is important since the evaluation of lesion composition could lead to reduce the biopsy examination, which at present is the only one able to establish the histological nature of the lesions, but it is invasive.

Recently, several clinical studies have been performed exploiting either frequency-domain or time-resolved optical instruments, both in reflectance and in transmittance geometry, aiming at the assessment of scattering and absorption properties of both the female breast and lesions, if present [5-15]. The characterization of breast lesions in terms of the main tissue constituents is also becoming the goal of some research studies, even if most still focus on the assessment of blood parameters since breast cancers are usually identified through the

detection of neovascularized areas that make tumors appear as strongly absorbing at red wavelengths. Studies on breast lesions have reported increased blood content in cancers [16-23] as compared to the surrounding normal tissue. Only in some studies, an extension of the spectral range was performed for the quantification also of water and lipids, since they are dominant constituents of the breast tissue. Up to know, preliminary studies on malignant breast lesions were performed, showing a reduction of lipid content and an increase of water and blood compared to normal breast tissue [24-30].

It is also emerging that another chromophore is important for the detection and characterization of breast lesions, that is collagen. It is in fact involved in the onset and progression of breast cancer [31,32], yet no optical study has been performed so far aiming at the assessment of collagen content in lesions.

In this work, we report on the preliminary results of a clinical study that enrolled more than 200 patients, based on multi-wavelength time-resolved transmittance measurements. A perturbation model based on the high-order calculation of the pathlength of photons inside the defect has been applied to retrieve the optical properties and the constituent concentration of a small inhomogeneity embedded in a homogeneous medium [33]. The *in vivo* characterization of malignant and benign breast lesions in terms of absorption properties and main constituents (blood, lipids, water and collagen) is presented. In particular a comparison is made in terms of absorption properties and tissue composition of both malignant and benign lesions with respect to the surrounding tissue in order to understand the capability to discriminate healthy and diseased breast tissue. Another goal of this study is the discrimination between malignant and benign lesions both in terms of absorption properties and tissue composition.

2. Instrument set-up

The instrument was designed to collect projection images in compressed breast geometry, in the same configuration as conventional X-ray mammography. Seven pulsed diode lasers are used as light sources emitting at 635, 680, and 785 nm (visible, VIS), and at 905, 930, 975 and 1060 nm (near-infrared, NIR), with average output power of ~1-5 mW, temporal width of ~150-400 ps and repetition rate of 20 MHz. The breast is softly compressed between parallel glass plates. The output light is collected on the opposite side of the compression unit by a fiber bundle, whose distal end is bifurcated, and its two legs guide photons respectively to a photomultiplier tube (PMT) for the detection of VIS wavelengths (R5900U-01-L16, Hamamatsu, Japan) and to a PMT for NIR wavelengths (sensitive up to 1100 nm, H7422P-60, Hamamatsu, Japan). Two PC boards for time-correlated single photon counting (TCSPC) are used for the acquisition of the seven time-resolved transmittance curves. The compressed breast is raster-scanned continuously, recording data every millimeter. A complete scan of one view typically requires 5 min. A detailed description of the set-up is reported in [34].

3. Data analysis

3.1 Homogenous model for bulk breast tissue characterization

Information on tissue composition and structure is obtained directly from time-resolved curves measured at 7 wavelengths. A spectrally constrained global fitting procedure [35], based on an analytical solution of the diffusion approximation (with the extrapolated boundary condition) for an infinite homogeneous slab [36,37], is applied. Free parameters of the fit are the concentrations of oxy- and deoxy-hemoglobin (HbO_2 and Hb, respectively), water, lipids, and collagen, together with the scattering amplitude a and power b. The Beer law is then used to estimate the absorption coefficient at each wavelength from the concentrations of the main tissue constituents. By the knowledge of the parameters a and b, the reduced scattering coefficient is modeled and obtained through a simple approximation to Mie theory: $\mu'_s = a(\lambda/\lambda_o)^{-b}$, where we set λ_o = 600 nm; in this way a is the interpolated scattering coefficient $\mu'_s(\lambda_o)$ [38,39].

For each breast view and wavelength, the estimate of bulk optical properties is limited to a reference area that excludes boundaries and marked inhomogeneities, but still includes most of the breast. To select that area, the mean time-of-flight (*i.e.* the first moment of the time-

resolved transmittance curve) is calculated for each image pixel, and only pixels with mean time-of-flight greater than or equal to the median of the distribution are included in the reference area, named matrix of time of flight (MTOF). The optical properties and the constituent concentrations of bulk tissue are then obtained as averages over the MTOF reference area. Examples of automatic MTOF selection are presented in Section 5.

3.2 Perturbation model for lesion characterization

In order to optically characterize breast lesions, we assume that they can be treated as localized absorption perturbations embedded in an otherwise homogeneous diffusive medium. The unperturbed and perturbed time-resolved transmittance curves, $T_0(t)$ and $T(t)$, respectively, can be linked exploiting the modified Lambert-Beer's law:

$$T(t) = T_0(t)\mathbf{e}^{-\Delta\mu_a l(t)}, \tag{1}$$

where $l(t)$ is the mean pathlength traveled in the inclusion by photons detected at time t, while $\Delta\mu_a$ represents the absorption variation inside the inclusion with respect to the unperturbed homogeneous background absorption $\mu_{a,0}$. The pathlength $l(t)$ can be derived as [40]:

$$l(t) = -\frac{1}{T_0(t)}\frac{\partial T_0(t)}{\partial \mu_a} \quad . \tag{2}$$

Equation (1) holds true in ideal conditions that is when the time response of the instrumentation is δ-like. We assumed that a similar relationship can be applied also when the experimental set-up has non-ideal temporal characteristics defined by its instrumental response function (IRF):

$$\widetilde{T}(t) = \widetilde{T}_0(t)\mathbf{e}^{-\Delta\mu_a \widetilde{l}(t)}, \tag{3}$$

where $\widetilde{T}_0(t)$ and $\widetilde{T}(t)$ are the unperturbed and perturbed time-resolved transmittance curves measured by the optical mammograph, while $\widetilde{l}(t)$ represents the photon pathlength traveled in the inclusion in this realistic case [42] and can be derived similar to Eq. (2):

$$\widetilde{l}(t) = -\frac{1}{\widetilde{T}_0(t)}\frac{\partial \widetilde{T}_0(t)}{\partial \mu_a} \quad , \tag{4}$$

The pathlength $\widetilde{l}(t)$ has been calculated by performing the numerical derivative reported in Eq. (4) exploiting an 8^{th} order perturbation method for deriving the expression of the time-resolved transmittance curve for a homogeneous medium with an inclusion inside [33].

Finally, we considered temporal binning of the measured time-resolved curves, in order to improve the signal-to-noise ratio. In particular, for this work data were analyzed dividing the transmittance curves in 10 equal-counts windows [41]. The 8^{th} window was then considered for the analysis to provide information on the absorption of the investigated medium, since it is related to late photons which are less affected by an eventual scattering variation inside the inclusion. Correspondingly, for the pathlength $\widetilde{l}(t)$ a similar binning procedure was implemented [42] and the equivalent gate was considered.

Then, from Eq. (3), the knowledge of the pathlength inside the inclusion allows one to calculate the absorption variation $\Delta\mu_a$ as:

$$\Delta\mu_a = -\frac{1}{l_{8^{th}}}\ln\left(\frac{T_{pert}}{T_{MTOF}}\right), \tag{5}$$

where T_{pert} and T_{MTOF} are the 8^{th} temporal windows of the experimental perturbed and background reference transmittance curves, respectively, while l_8^{th} is mean pathlength traveled inside the inclusion by photons detected at the 8^{th} temporal window.

The background unperturbed curve is obtained as an average over the MTOF that excludes boundaries and marked inhomogeneities (as reported in Sec 3.1). The experimental perturbed curve is obtained from an area centered on the corresponding inhomogeneity (*i.e.* lesion) position. The area size strictly depends on the lesion size. For lesion diameters >15 mm, an area of 9x9 mm^2 was selected, otherwise 5x5 mm^2.

Starting from $\Delta\mu_a$ and knowing the extinction coefficient of the main constituents of breast tissue, by the Beer law we can estimate the variation of the concentrations ΔC_i between lesion and background tissue (in terms of blood, water, lipid and collagen).

The perturbation method adopted here relies on the *a priori* knowledge of the volume and location of the inhomogeneity. We have always assumed a spherical inhomogeneity located at halfway between source and detector. For the size, we considered an equivalent sphere based on the maximum diameter of the lesion obtained by histopathology, when available, or by RX or US elsewhere.

3.3 Data analysis for imaging

A dedicated software, written in the Matlab environment (R2010, The Mathworks Inc. Natick, USA), is used to create images of the absorption variation ($\Delta\mu_a$ maps) between an eventual lesion located at pixel (*x,y*) and the healthy tissue. Similarly to Eq. (5), the absorption variation in each pixel is derived as:

$$\Delta\mu_a(x,y) = -\frac{1}{l_{8^{th}}}\ln\left(\frac{T_{pert}(x,y)}{T_{MTOF}}\right). \quad (6)$$

The aim of the $\Delta\mu_a$ maps is to highlight the difference between the lesion and the surrounding tissue in terms of the absorption at the 7 wavelengths. Moreover, starting from the $\Delta\mu_a$ maps and considering the Beer law, it is possible to reconstruct the concentration variation maps (ΔC_i maps) between lesion and healthy tissue in terms of breast constituents (*i.e.*, oxy- and deoxy-hemoglobin, lipids, water and collagen).

4. Clinical study

From June 2009 to January 2014, 218 subjects (mean age 51 years, age range 19-79 years) were enrolled in the clinical study. The Institutional Review Board at the European Institute of Oncology (Milan, Italy) approved the study and written informed consent was obtained from all the participants.

The clinical study had twofold aim: the non-invasive assessment of breast density by optical means (not considered here) [43,44], and the optical characterization of malignant and benign lesions.

Optical images were routinely acquired from both breasts in cranio-caudal (CC) and oblique (OB, 45◦) views, to allow easy comparisons with the X-ray mammograms, typically available in the same views for all patients.

So far we have performed the full analysis for 62 patients for which the complete clinical information is available (mean age 51 years, age range 21-79), each bearing a lesion. In particular, 33 patients with a malignant lesion and 29 with a benign lesion were analyzed.

A retrospective study was performed and optical images were analyzed comparing them to X-ray mammograms acquired in the same views. After data analysis of the homogeneous area of the breasts included in the dataset for this study, 1 out of the 33 malignant cases and 1 out of the 29 benign ones were excluded from further analysis for lesion characterization, because of the weak signal that caused problems to the fitting procedure. Fifteen out of the 32 malignant cases and 16 out of the benign ones were analyzed only in one view (either CC or

OB), because they were not clearly detected in the other view. The number and type of lesions included is reported in Table 1.

Table 1: Types and number of lesions included in the study

Lesion type	**N°**	**Lesion nature**
Ductal invasive carcinoma	26	Malignant
Lobular invasive carcinoma	2	Malignant
Mucinous invasive carcinoma	2	Malignant
Intraductal carcinoma DIN 2 (middle grade)	2	Malignant
Fibroadenoma	9	Benign
Phylloides tumor	3	Benign
Papilloma	3	Benign
Cyst	2	Benign
Fibrocystic proliferative disease	2	Benign
Fibrolipoma	2	Benign
Fibroadipose nodule	1	Benign
Parenchymal fibrosis	1	Benign
Ductal hyperplasia	1	Benign
Surgery scar	1	Benign
Others	3	Benign

As reported in Table 1, there are several types of both malignant and benign lesions. For data analysis, due to the limited frequency of each type, all the benign lesions were grouped in a single category, named 'Benign' and all the malignant in another one, named 'Malignant'.

5. Results and discussion

The goal of this study is to assess *in vivo* by optical means the spectral absorption properties and the composition of malignant and benign breast lesions in order to understand if these pieces of information allow one to distinguish diseased tissue from healthy one, and to discriminate between malignant and benign lesions.

5.1 Imaging

An example of $\Delta\mu_a$ maps at the 7 wavelengths is shown in Figure 1, together with the X-ray image of the CC view of the left breast of a patient (#13) with a phylloides tumor (benign) of 45 mm in the upper-outer quadrant. This type of lesion is considered as atypia and has a very rapid growth. It is a fibro epithelial tumor with an epithelial and a cellular stromal component.

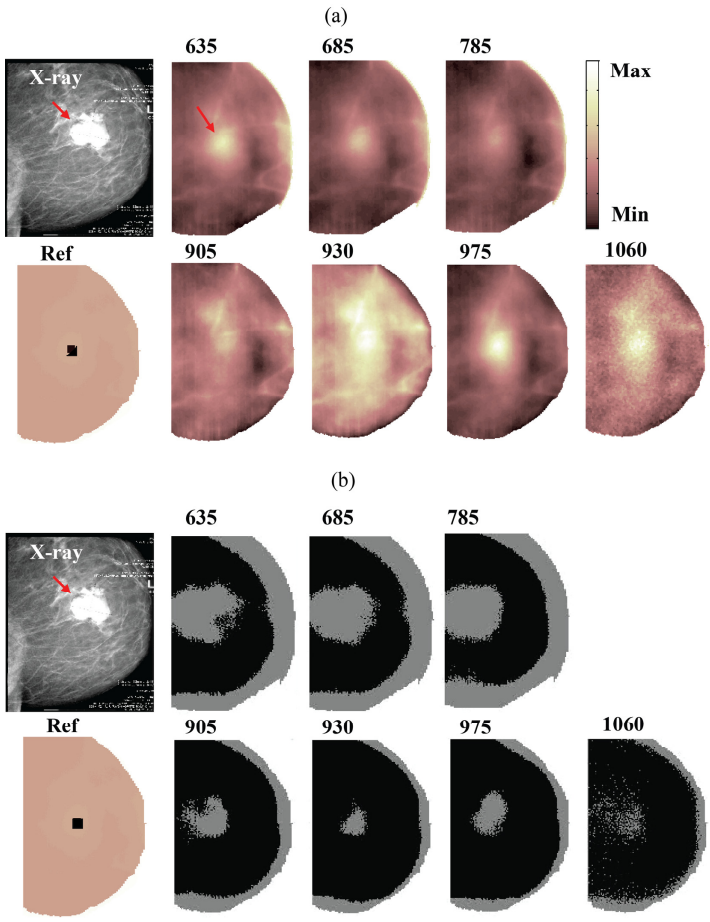

Fig. 1. (a) X-ray image (top left) and $\Delta\mu_a$ maps at the 7 wavelengths of the left CC view of the patient #13 with a phylloides tumor of 45 mm in the upper-outer quadrant. A reference image showing the selected lesion area is also reported (bottom left). The color bar range (cm^{-1}) for $\Delta\mu_a$ maps is -0.06 to 0.25 (635 nm), -0.04 to 0.23 (685 nm), -0.02 to 0.12 (785 nm) , -0.02 to 0.04 (905 nm) , -0.02 to 0.02 (930 nm) , -0.02 to 0.08 (975 nm) , -0.02 to 0.04 (1060 nm). (b) Corresponding MTOF reference background area at the 7 wavelengths. A red arrow points to the lesion location. Compressed breast thickness 5.5 cm.

The lesion area, selected based on the criteria mentioned in Section 3.2, is also displayed at the bottom left of Figure 1. Moreover, images representing the MTOF reference background area of the same breast are reported in Figure 1(b), showing that it corresponds to most of the breast, but excludes boundaries and marked inhomogeneities.

In general, all $\Delta\mu_a$ maps show different absorption properties between the lesion and the healthy tissue at the 7 wavelengths. The tumor is evident with a good contrast at short wavelengths (635-685 nm), suggesting a high blood content. Good contrast is achieved also at 975 nm and 1060 nm and can be ascribed to the fibrous nature of the lesion that implies high water and collagen content and is evident as radiopaque tissue in the X-ray image. Even if with lower contrast, the tumor is also detected at 905 and 930 nm. The tumor area has different shape and extension at different wavelengths, It is possible to note a double clear area at 905, 930 nm and 1060 nm, whereas only one clearer area at 975 nm in the lower region of the lesion. This is due to the different nature tumor composition.

ΔC_i maps of the same lesion, representing the concentration variations of oxy- and deoxy-hemoglobin, lipids, water and collagen between the tumor and the healthy tissue, are reported in Figure 2.

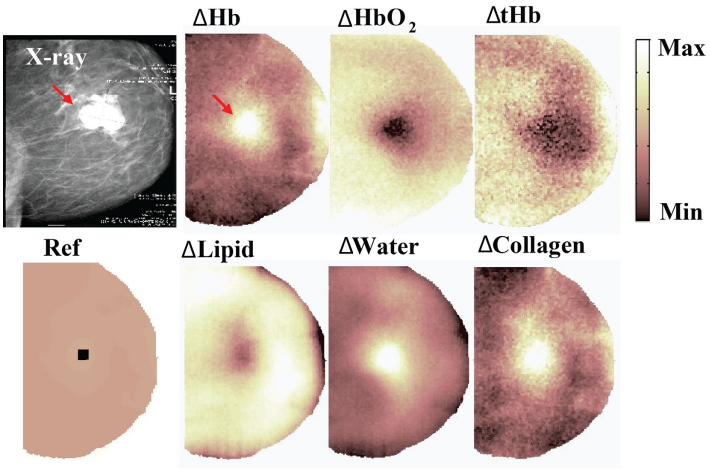

Fig. 2. X-ray image (top left) and ΔC_i maps of the main breast constituents (Hb, HbO_2, tHb, lipid, water and collagen) of the left CC view of the patient #13 with a phylloides tumor of 45 mm in the upper-outer quadrant. A reference image showing the selected lesion area is also reported (bottom left). A red arrow points to the lesion location. The color bar range for ΔC_i maps is -2.9 to 8.4 (ΔHb(μM)), -12.6 to 6.6 (ΔHbO_2(μM)), -6.2 to 6.0 (ΔtHb (μM)), - 240.4 to 77.3 (ΔLipid(mg/cm^3)), -35.6 to 87.1 (ΔWater(mg/cm^3)), -74.7 to 187.2 (ΔCollagen (mg/cm^3)).

Higher hemoglobin, water and collagen content in the lesion area with respect to the surrounding healthy tissue, and lower oxy-hemoglobin and lipid content are estimated. This is compatible with the lesion nature, since the phylloides tumor can contain blood and has a stromal component. ΔC_i maps confirm the heterogeneous composition of the lesion, which appears smaller when blood and water are considered, and wider in the lipid (and perhaps collagen) map.

Figure 3 shows $\Delta\mu_a$ maps at the 7 wavelengths together with the X-ray image of the CC view of the left breast of a patient (#99) with a 25 mm invasive ductal carcinoma (malignant) in the retroareolar region.

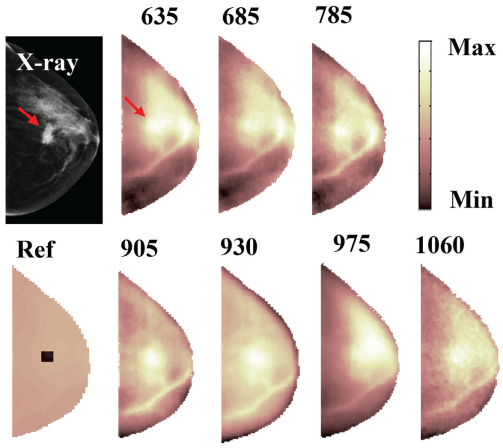

Fig. 3. X-ray image (top left) and $\Delta\mu_a$ maps at the 7 wavelengths of the left CC view of patient #99 with a 25 mm invasive ductal carcinoma in the retroareolar area. A reference image showing the selected lesion area is also reported (bottom left). A red arrow points to the lesion

location. The color bar range (cm^{-1}) for $\Delta\mu_a$ maps is -0.06 to 0.09 (635 nm), -0.04 to 0.06 (685 nm), -0.03 to 0.05 (785 nm), -0.06 to 0.06 (905 nm), -0.13 to 0.09 (930 nm), -0.11 to 0.22 (975 nm), -0.06 to 0.08 (1060 nm).

A clear white area corresponding to the lesion is observed at each wavelength. The mammary gland is also characterized by strong absorption at 635-785 nm and at 975-1060 nm. On the contrary, strong diffuse absorption at 930 nm indicates that the breast tissue is generally fatty. In fact, in the X-ray image the lesion and the gland are radiopaque (fibrous), while the surrounding tissue is translucent (adipose). A blood vessel is also clearly visible in both optical and radiological images.

The corresponding ΔC_i maps of the same breast are reported in Figure 4.

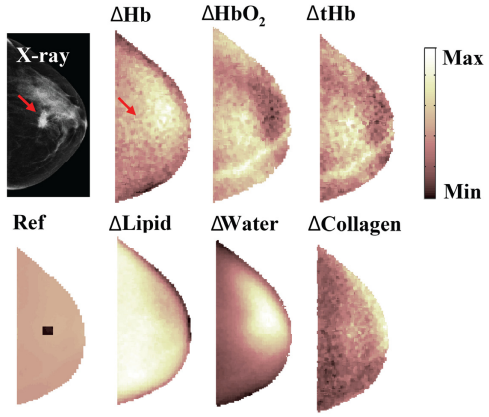

Fig. 4. X-ray image (top left) and ΔC_i maps of the main breast constituents (Hb, HbO_2, tHb, lipid, water and collagen) of the left CC view of the patient #99 with an invasive ductal carcinoma of 25 mm in the retroareolar area. A reference image showing the selected lesion area is also reported (bottom left). A red arrow points to the lesion location. The color bar range for ΔC_i maps is -5.2 to 7.0 (ΔHb(μM)), -12.0 to 10.1 (ΔHbO_2(μM)), -10.5 to 12.7 (ΔtHb (μM)), - 905.9 to 181.5 (ΔLipid(mg/cm^3)), -164.5 to 44.8 (ΔWater(mg/cm^3)), -101.2 to 261.8 (ΔCollagen (mg/cm^3)).

A slight increase can be appreciated in the total hemoglobin content (due in particular to an increase in the oxy-hemoglobin content) in the lesion area with respect to the surrounding tissue. Similarly, the blood vessel is clearly identified by a high *tHb* value due to high HbO_2 content. Slightly higher collagen content can be also seen at the lesion location. In the water map only a large white area corresponding to higher water content can be observed, probably due to the presence of the mammary gland that masks the closely located tumor.

5.2 Comparison of absorption and tissue composition between malignant and benign lesions

As first step we tried to discriminate diseased from healthy tissue. We statistically quantified the differences in terms of absorption between malignant and benign lesions and corresponding healthy tissue using the Wilcoxon test. Table 2 reports the corresponding *p*-values.

Table 2. *p*-value of the Wilcoxon test for $\Delta\mu_a$ of either benign or malignant lesions *vs* healthy tissue

	Wavelength(nm)						
	635	**685**	**785**	**905**	**930**	**975**	**1060**
***p*-value** Benign lesion	0*	0	0	0.004	0.4	0.006	0.004
***p*-value** Malignant lesion	0	0	0	0	0	0	0

*Any $p < 10^{-4}$ is reported as $p = 0$.

From Table 2, the absorption difference with respect to healthy tissue is statistically significant ($p < 0.05$) for both benign and malignant lesions at all wavelengths, except for benign lesions at 930 nm. These results show a significant discrimination between diseased tissue and healthy one, suggesting the absorption variation as a good parameter for diagnostic purposes.

Among women a wide variability of breast tissue absorption properties can be observed. Since $\Delta\mu_a$ refers the absorption properties of the lesion to those of the surrounding healthy tissue, it can also account for the inter-subject variability of the background tissue when evaluating the optical differences between malignant and benign lesions.

Figure 5 reports the $\Delta\mu_a$ of both malignant and benign lesions at the 7 wavelengths.

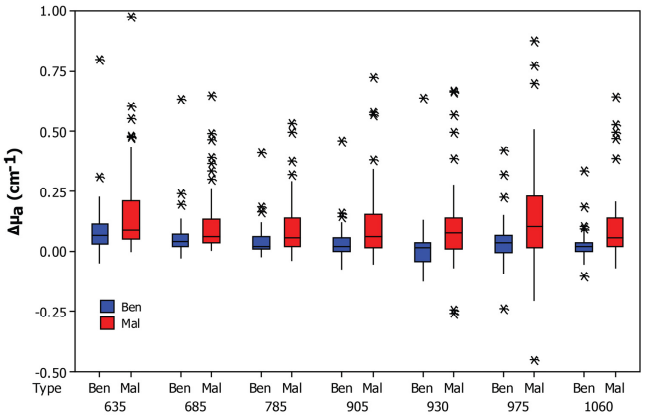

Fig. 5. Comparison of the absorption variation $\Delta\mu_a$ for both malignant and benign lesions at the 7 wavelengths. For a better data visualization, the lower limit of the y-axis was rescaled to -0.5, excluding one outlier.

On average malignant lesions have higher absorption variation with respect to benign ones in the whole spectral range. In order to quantify the differences between the two lesion categories, Table 3 reports the *p*-values obtained by the Mann-Whitney test when comparing the absorption variation for malignant versus benign lesions.

Table 3. *p*-value obtained by Mann-Whitney test for $\Delta\mu_a$ between benign and malignant lesions

	Wavelength (nm)						
	635	**685**	**785**	**905**	**930**	**975**	**1060**
***p*-value**	0.11	0.05	0.004	0.008	0.004	0.02	0.003

Significant *p*-values are obtained from 785 to 1060 nm. In particular the difference is marked at 785 nm, where usually oxy-hemoglobin absorption is dominant, and at 1060 nm, where collagen absorption has the highest relative weight. Moreover a statistically important discrimination is achieved at 930 nm, where there is the absorption peak of lipid.

For what concerns the constituent concentrations, the differences between both lesion types and the corresponding healthy tissue were also statistically quantified. This parameter allows us to estimate which constituents are more involved in diseased tissue, and in particular if there are different concentrations between malignant and benign lesions. Table 4 reports the corresponding *p*-values.

Table 4. *p*-value obtained using the Wilcoxon test for ΔC_i of benign and malignant lesions

	ΔConstituents					
	Hb (μM)	**HbO_2 (μM)**	**tHb (μM)**	**Lipid (mg/cm^3)**	**Water (mg/cm^3)**	**Collagen (mg/cm^3)**
***p*-value** Benign lesion	0	0.87	0.003	0.001	0.01	0
***p*-value** Malignant lesion	0.002	0.004	0	0.003	0.02	0

Significant *p*-values are obtained for both malignant and benign lesion groups for all the constituent chromophores, except for the oxy-hemoglobin for benign lesions. These results indicate that there are significant variations in terms of composition between diseased tissue and healthy one.

The correlation between malignant and benign lesions was also performed in terms of constituent concentration variation ΔC_i, as reported in Figure 6.

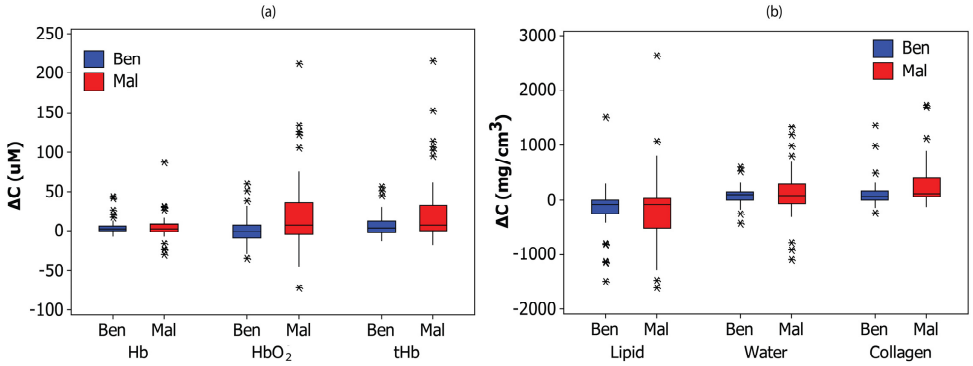

Fig. 6. Constituent concentration variation ΔC_i of blood parameters (a) and lipid, water and collagen (b) for malignant (red) and benign (blue) lesions.

Figure 6(a) confirms the higher blood concentration in both malignant and benign lesions with respect to the healthy tissue. Moreover, difference in terms of blood concentration is observed between malignant and benign lesions. In particular, oxy-hemoglobin is present in higher amount in malignant lesions with respect to benign ones, and that also yields higher total hemoglobin content. This result is consistent with tumor volume being characterized by high vascularization. For what concerns the other main constituents of breast tissue, for both lesion types higher collagen and slightly higher water content is observed, together with slightly lower lipid content. For all constituents, the concentration difference is more marked for malignant lesions than for benign ones. For the first time collagen concentration has been

quantified, allowing a more complete characterization of the tumor tissue constituents. Actually, among the three major constituents, the most significant variation occurs for collagen. This result is in agreement with observations reported in the literature since collagen is involved in the onset and progression of breast cancer [32]. Thus the quantification of collagen content in breast lesions with respect to the surrounding healthy tissue might have diagnostic relevance.

In order to evaluate if also the differences between malignant and benign tissue are statistically significant, the Mann-Whitney test was applied to ΔC_i values obtained for malignant and benign lesions. Table 5 reports the corresponding *p*-values.

Table 5. *p*-value obtained by Mann-Whitney test for ΔC_i between benign and malignant lesions

	ΔConstituents					
	Hb (uM)	**HbO_2 (uM)**	**tHb (uM)**	**Lipid (mg/cm^3)**	**Water (mg/cm^3)**	**Collagen (mg/cm^3)**
***p*-value**	0.9	0.04	0.05	0.7	0.6	0.01

Significant *p*-values are obtained for oxy-hemoglobin and collagen. This suggests that benign and malignant lesions could potentially be discriminated on the basis of these two constituents, even if the difference is not highly significant. These results could be relevant for the discrimination of benign and malignant lesions since they are in line with what is known from pathology, namely that the development of breast cancer tissue involves neo-angiogenesis and the presence of a marked stromal component, rich in collagen.
It can be observed from data reported in this paragraph that the discrimination between benign and malignant breast lesions is less significant if the constituent concentrations variation instead of the absorption variation is considered.

5.3 Study limitations

The data analysis procedure by means of the perturbation model presented here has some critical aspects. They mainly concern geometrical assumptions in the perturbation model and the assessment of lesion volume.

As mentioned in Section 3.2, the perturbation model relies on the *a priori* knowledge of the volume and location of the inhomogeneity, which is always assumed as spherical, since only one dimension (*i.e.*, the maximum diameter) of the lesion is known, and located halfway between the injection and detection points.

As studied elsewhere in the case of a totally absorbing lesion, assuming the same volume, the dependence on the shape of the lesion is negligible when the three dimensions are similar as in the case of a sphere and of a cylinder with equal height and diameter [45]. We have not studied yet the case of large differences in dimensions.

Imaging by optical means might detect composition variations corresponding to a bigger area than the real tumor volume, leading to show a bigger diseased area. This could happen if vascularization were not strictly limited to the tumor location, but extended beyond it. We need to understand if this aspect has to be taken into account for the correct assessment of the lesion volume.

Errors on the volume size lead to errors in the estimation of $\Delta\mu_a$ and consequently of ΔC_i. In the limit of small perturbation where the model used in the present study approaches the Born approximation, the relative uncertainty on the volume is reflected in a corresponding relative uncertainty on the absorption change, since the optical perturbation is related to the product of $\Delta\mu_a$ and the lesion volume. Therefore it affects the absolute absorption values, but not the $\Delta\mu_a$ line shape. For larger changes, the dependence on the volume is non-linear, and cannot be factorized as a constant term for all wavelengths, thus it can somehow affect also relative concentrations changes.

Another limitation of the model is that information on the lesion depth was not available, so it was located halfway between source and detector. Thus the effect of an incorrect assumption on the lesion depth on the estimation of the optical properties and constituent concentrations should be investigated.

6. Summary and conclusions

The in vivo characterization of malignant and benign breast lesions was performed in terms of both optical properties and main constituents of breast tissue, that are blood, lipids, water and collagen. In particular, a total of 62 lesions were analyzed, including 33 malignant and 29 benign lesions. For what concerns spectral changes in optical properties, a relevant variation was observed at 785 nm where oxy-hemoglobin has strong absorption and at 1060 nm where collagen absorption is marked. Moreover a statistically important discrimination can be seen at 905 and 930 nm where there is the peak of lipid.

For what concerns changes in tissue constituents, the lesion area is characterized by a higher amount of oxy-hemoglobin and collagen with respect to the healthy tissue and a decrease of the lipid content. This trend can be observed for both benign and malignant lesions, but also significant differences are obtained between the two lesion categories. In fact, they can be statistically discriminated on the basis of oxy-hemoglobin and collagen content. These results could be relevant for the discrimination of benign and malignant lesions since they confirm what is known from the patho-physiological point of view, namely that breast cancer is a strongly vascularized tissue and is characterized by the presence of a stromal structure, in which collagen is involved. Up to now, collagen has never been considered for the characterization of breast lesions. Collagen contribution to the tumor characterization might prove important, since it is involved in the development of the breast cancer.

Preliminary results reported here refer to group analysis showing that from the statistical point of view there is a good potential for lesion detection and characterization both in terms of absorption properties and constituent concentrations, while it is less straightforward the discrimination between benign and malignant tumor. For this reason, the classification of breast lesions on an individual basis will be tested at the end of the whole study, when enough data are available for a more robust conclusion. Moreover, up to now, all lesions were grouped in two classes, benign and malignant, although this classification gathers lesions that are quite diverse, such as cysts and fibroadenomas for what concerns the benign category. A further analysis to be performed with larger numbers will aim at identifying more homogeneous lesion classes.

Acknowledgements
The research leading to these results has received funding from LASERLAB-EUROPE (grant agreement n° 284464, EC's Seventh Framework Programme). We would like to thank Dr. Fabrizio Martelli, Department of Physics, Università degli Studi di Firenze, for providing the numerical routines for the perturbation model and for many useful discussions.